J. Fluid Mech. (1996), vol. 319, pp. 251–279

Initial streamwise vorticity formation in a two-stream mixing layer

By STEVE TUNG† AND STANLEY J. KLEIS
Department of Mechanical Engineering, University of Houston, Houston, TX 77204, USA

(Received 27 April 1993 and in revised form 22 March 1996)

The characteristics of the initial formation of streamwise vortices and their relation to the spanwise structures are experimentally investigated at several phases of the initial roll-up and pairing in a two-stream mixing layer at high Reynolds numbers (up to $Re_\theta = 1.25 \times 10^3$). The spanwise structures were stabilized by acoustically exciting the mixing layer at the natural instability frequency and its first subharmonic. No artificial spanwise forcing was applied. Quantitative information was obtained through conditional sampling with the forcing signal as the phase reference. Time traces of the three velocity components were recorded by hot-wire anemometry at a grid of locations on planes normal to the flow at four successive streamwise locations which include the roll-up and first pairing of the spanwise structures. From these measurements, three-dimensional distributions of ensemble-average vorticity components were computed and analysed.

The results show that the spanwise structures remain mostly two-dimensional from roll-up to the end of the first pairing, except for small oscillations in curvature of their axes. Concentrated streamwise vortices evolve at locations corresponding to small 'kinks' in the spanwise rollers and first appear at the beginning of the pairing process. Their subsequent development bears many similarities with the results of small-perturbation simulations. They expand laterally, forming counter-rotating rib vortices that grow almost exponentially in the braid region. In the core region, a complex but organized streamwise vorticity pattern emerges. The pattern consists of layered streamwise vortices whose orientation suggests that the oscillation of the spanwise roller core is π radians out of phase with that of the streamwise vortex lines that join the rib vortices. The peak streamwise vorticity and circulation in the core region increase until the completion of the spanwise structure pairing when the layered pattern collapses. Measurements at large spanwise locations conducted downstream show that the 'kink' is not the only location of streamwise vorticity generation: streamwise vortices develop at nearly periodic spanwise locations other than that of the initial 'kink'. The initial spacing between streamwise vortices agrees with previous stability analysis. At the end of the spanwise structure pairing, isolated pairings between streamwise vortices take place, but a global doubling in spanwise wavelength does not occur.

1. Introduction

Organized streamwise vortices (structures with concentrated streamwise vorticity) in boundary-free plane mixing layers have been the subject of extensive investigation

† Present address: UCLA MAE Department, 48-121 ENGI IV, Box 951597, Los Angeles, CA 90095-1597, USA.

in recent years. Experimentally, some of the more successful works to date have been in flow visualizations (Breidenthal 1981; Bernal & Roshko 1986; Lasheras, Cho, & Maxworthy 1986; Lasheras & Choi 1988; among others). Through the distribution of passive scalars such as smoke and dye, visualization pictures demonstrate the existence of organized streamwise structures in the braid region between the rolled-up spanwise vortices. These structures appear to be stationary in space and form a continuous vortex line that travels back and forth between successive spanwise rollers (Bernal & Roshko 1986). The interest in the streamwise structures results from the hypothesis that they are the link between the initial two-dimensional base flow and the downstream three-dimensional turbulence. This idea is supported by the observation that the streamwise vortices trigger the production of small scales which are the main ingredient of turbulent flows (Konrad 1976; Huang & Ho 1990).

Stability studies (Pierrehumbert & Widnall 1982; Corcos & Lin 1984) suggested that the streamwise structures are the result of a three-dimensional instability of the mixing layer. However, it is not yet clear whether the formation mechanism is associated with the braid region or the roller core itself.

Numerical simulations of the mixing layers (Metcalfe *et al.* 1987; Ashurst & Meiburg 1988; Rogers & Moser 1992, 1993; Moser & Rogers 1993) have been successful in computing the details of the three-dimensional structures. In addition to mapping the streamwise vortices in the braid region, the simulations also provide a glimpse into the complex core (region) flow during merging of the spanwise structures.

Compared to flow visualization studies and numerical simulations, quantitative experiments that measure the physical quantities of the streamwise structures are scarce. This is mainly due to the many technical difficulties associated with conducting such experiments. For example, the experimental time required to obtain all three velocity components in a three-dimensional space is extremely long, during which the equipment output can drift to unacceptable levels. In addition, the small-scale nature of the streamwise structures poses a severe spatial resolution problem for most experimental facilities. A number of studies have been carried out to obtain the 'indirect' measurements associated with the streamwise structures. Among them, Jimenez (1983) measured the time-average spanwise velocity distribution of a square jet; Huang & Ho (1990) measured 'partial' streamwise vorticity in an acoustically excited mixing layer. Nygaard & Glezer (1991) studied phase-averaged r.m.s. velocity fluctuations of coherent three-dimensional structures in a thermally excited water channel. They showed that undulations of the spanwise rollers developed only when the spanwise excitation wavelength exceeded the initial two-dimensional instability (Kelvin–Helmholtz) wavelength. Recently, Bell & Mehta (1989,1992) conducted a fine-scale mapping of the streamwise structures. Their time-average results represent one of the few measurements of a streamwise vorticity distribution in a mixing layer.

The present study was designed to further quantify the streamwise structures on a phase-averaged basis. Experiments were carried out to obtain the necessary information to reconstruct a three-dimensional picture of the phase-averaged streamwise vortices in a two-stream mixing layer. The flow field was acoustically excited at the combined frequency of the initial instability mode and its first subharmonic to reduce phase jittering and provide an organized two-dimensional base flow for the evolution of 'natural' three-dimensional structures. No artificial spanwise forcing was included so that the emergence of a preferred wavelength could be identified. All three velocity components were measured by hot-wire anemometry on a three-dimensional grid of locations. Conditional sampling, using the forcing frequency as a phase reference, was set up to acquire phase-aligned velocity time traces. The velocity time series were en-

semble averaged and the corresponding three-directional vorticity distributions were computed and analysed. Taylor's hypothesis with a constant convection velocity was used to estimate the spatial distributions of velocity near the physical locations of measurement.

2. Experimental facility and conditions

All experiments in the present study were conducted in the large two-stream mixing layer facility located in the Turbulent Shear Flow Laboratory of the University of Houston. The facility is designed to provide a low-noise environment for quantitative studies of a large-scale incompressible mixing layer. The facility consists of three main components: a dual-fan low-speed wind tunnel, a splitter plate with boundary layer control, and a three-dimensional traversing system. The wind tunnel is of a closed-loop design. A schematic diagram of the mixing layer facility is provided in figure 1(*a*). A splitter wall separates the main channel into two almost identical chambers. Air flows in the chambers are independently driven by two axial flow fans. Maximum flow rate attainable is about 30 m s^{-1}. To minimize free-stream turbulent fluctuations, five layers of fine mesh wire screens and a six to one contraction were installed upstream of the test section. Typical r.m.s. velocity fluctuation levels in the free-stream region of the test section are about 0.07 % of the mean flow. The cross-sectional area of the test section is 1.05 m by 1.65 m. The test section extends 12 m in the streamwise direction. Preceding the test section, the last portion of the splitter wall of the wind tunnel is fitted with a specially designed splitter plate or 'knife-edge' which has boundary layer control capability. By using boundary layer suction, laminar boundary layers can be maintained up to a free-stream velocity of about 10 m s^{-1}. A schematic of the knife-edge can be found in figure 1(*b*).

A three-coordinate traversing system allowed automated hot-wire positioning in the mixing layer. To minimize flow interference, the entire system was installed outside the wind tunnel, except for a 2.54 cm diameter stainless steel tubing that runs vertically through the ceiling of the tunnel into the test section. A TSI Model 1155-18 probe support was attached perpendicular to the end of the tubing, allowing the hot-wire probe to be located about 45 cm upstream from the tubing. Traverse movement in all three directions was free of backlash with a resolution of 0.0254 mm. This was carried out by ball-bearing lead-screws driven by stepping motors which were under the control of a MASSCOMP laboratory computer system.

Velocity measurements were performed by constant-temperature hot-wire anemometry with a TSI T1.5 x-wire. The wires were connected to a TSI IFA-100 Intelligent Flow Analyzer with an overheat ratio of 1.4. Analog signals from the hot-wire anemometers were digitized by the A/D converter of the MASSCOMP computer. The converter consists of 16 channels with a resolution of 12 bits for an input voltage range from -10 to $+10$ V. The computer is equipped with five programmable clock modules which allow synchronization of the conditional sampling activities in the current study. Hot-wire calibration was carried out in the free-stream region of the wind tunnel, where the only non-zero velocity component was in the streamwise direction. Output from the x-wire was calibrated against velocity data measured by a Pitot tube. Based on the error of the calibration procedure and the scale of the x-wire, the accuracy of the ensemble-average streamwise velocity, $\langle u \rangle$, is estimated to be within 5%; the accuracy of the ensemble-average transverse and spanwise components, $\langle v \rangle$ and $\langle w \rangle$, is estimated to be 10%. As pointed out by Bell & Mehta (1989), in a flow field where a transverse gradient of the streamwise velocity exists, the separation

(a)

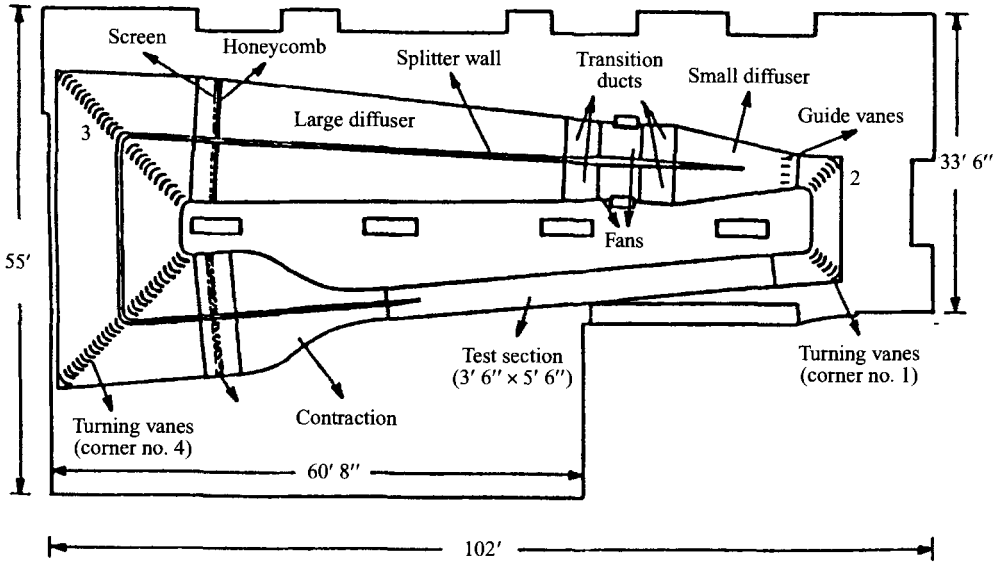

(b)

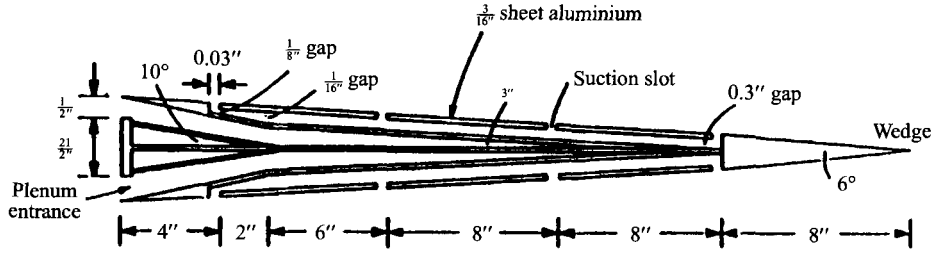

FIGURE 1. A schematic diagram of the experimental setup: (*a*) the wind tunnel; (*b*) cut-away view of the splitter plate (knife-edge).

between the two sensor wires of an x-wire probe will generate a pseudo-quantity in the spanwise velocity measurement. The correction scheme that they used, which was based on removing the contribution from the mean transverse velocity gradient, was also applied to the present spanwise phase-averaged velocity data.

For the majority of the measurements, the mixing layer was acoustically excited at low amplitude to minimize phase jittering and provide a phase reference for conditional sampling. The acoustic wave was generated by a loudspeaker which consisted of a 12 in. sub woofer. The speaker was located about 5 m downstream from the trailing edge of the knife-edge. It was found that, due to the closed-loop nature of the wind tunnel, the efficiency of acoustic excitation was high regardless of the exact location of the speaker. The forcing frequency was a linear combination of the initial instability frequency and its first subharmonic (= 130 and 65 Hz, respectively). The fundamental component was included to stabilize the roll-up of the mixing layer and the first subharmonic was used to stabilize the first pairing of the spanwise vortices (Ho & Huang 1982). For the free-stream velocity combination adopted in the present study (see below), the fundamental frequency corresponds

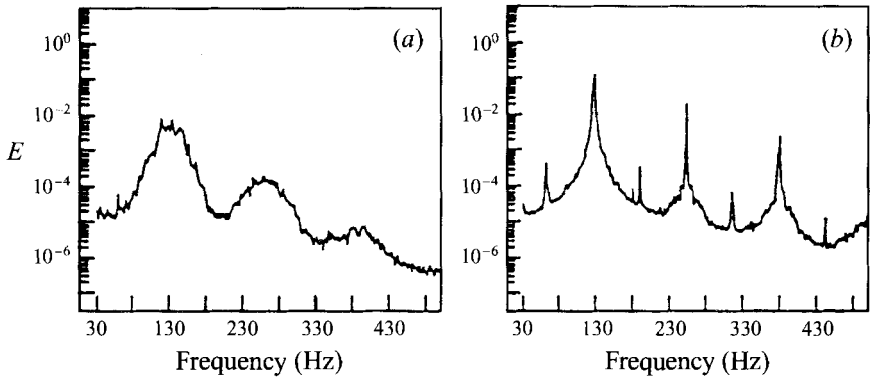

FIGURE 2. Power spectra of hot-wire signal measured at $x = 7.5$ cm and $y = -0.5$ cm. (*a*) unforced mixing layer; (*b*) forced mixing layer.

to a streamwise wavelength of 2.8 cm (λ_0). The two frequency components had identical amplitudes with a relative phase shift of 0.6π radians which was maintained throughout the experiment by a Wavetek Model 186 phase-lock generator. This phase shift ensured that pairings instead of shreddings of the spanwise structures take place in the mixing layer (Riley & Metcalfe 1980). The lowest level of the acoustic wave that caused the initial instability of the mixing layer to phase-lock to the forcing signal was chosen to be the forcing level. This level corresponds to about 0.05% of the dynamic pressure based upon free-stream velocity difference, ΔU. The uniformity of the acoustic forcing was checked by a microphone along the trailing edge of the splitter plate. The variation in intensity and phase was found to be less than 10% over the entire span and 2% over the span where measurements were taken. Figure 2 demonstrates the difference in u' power spectra between the excited and unexcited mixing layer. The single-wire probe used to measure these data was positioned at $y = -0.5$ cm and $x = 7.5$ cm. The acoustic excitation successfully suppressed phase jittering in the initial stage of the mixing layer instability as evidenced by the presence of 'spikes' instead of 'humps' in the u' spectra. The velocity fluctuation in the mixing layer became phase-locked to the forcing signal throughout the roll-up and first pairing of the spanwise structures. Successive stages of roll-up and pairing were observed to take place at fixed streamwise locations (Huang & Ho 1990). The effect of the acoustic forcing on the development of the mean flow is discussed in § 5.

An automated conditional sampling procedure was designed to acquire phase-dependent time records from the hot-wire anemometers. The first subharmonic part of the acoustic forcing signal was used as the phase reference. The same phase shift between the fundamental and the first subharmonic modes (0.6π radians) was used for all measurements. The TTL pulse train, generated by the phase-lock generator, served as the triggering signal for the A/D converter. At the rising edge of a pulse, the converter sampled a time trace from each of the two hot-wire anemometers after a preset time delay. The sampling rate used was 4000 samples per second. Each time trace consisted of 100 to 150 data points which corresponded to 25 to 37.5 ms in sampling time. At these sampling conditions, information from at least two spanwise structures and their surroundings was included in the time records. At each location of measurement, 100 phase-coherent time traces were recorded. Conditional sampling was carried out on a two-dimensional grid of locations in the (y, z)-plane at four streamwise stations: $x = 7.62$, 15.24, 22.86, and 26.67 cm. Details of the exact

Streamwise location(cm)	Transverse dimension(cm)	Spanwise dimension(cm)	Grid dimension	Grid size (mm × mm)	Grid size/λ_0
7.62	−2.54 to +2.54	−5.08 to +5.08	21 × 24	2.54 × 2.54	0.091 × 0.091
15.24	−2.54 to +2.54	−5.08 to +5.08	21 × 24	2.54 × 2.54	0.091 × 0.091
22.86	−3.81 to +3.81	−5.08 to +5.08	31 × 41	2.54 × 2.54	0.091 × 0.091
26.67	−2.54 to +5.08	−10.16 to +10.16	31 × 81	2.54 × 2.54	0.091 × 0.091

TABLE 1. Locations of phase-coherent measurements

locations of measurements are documented in table 1. The conditionally sampled velocities were ensemble-averaged based on the double decomposition formulation. The theoretical background of the decomposition can be found in Hussain, Kleis, & Sokolov (1980) and ?. The three components of ensemble-average vorticity, $\langle\omega_x\rangle$, $\langle\omega_y\rangle$, and $\langle\omega_z\rangle$, were computed using centre-differencing from the ensemble-average velocities. The estimated uncertainty for the streamwise component is 25%. In computing the spatial derivatives, Taylor's hypothesis was used to obtain the derivatives in x from the temporal derivatives such that

$$\frac{\partial}{\partial x} = -\frac{1}{U_c}\frac{1}{\partial t} \tag{2.1}$$

where U_c is the mean convection velocity of the mixing layer. Note that the use of Taylor's hypothesis affects the calculation of $\langle\omega_y\rangle$, and $\langle\omega_z\rangle$, but not $\langle\omega_x\rangle$, which includes no derivative in the streamwise direction. The $\langle\omega_z\rangle$ distribution, as will be demonstrated, is dominated by the large-scale spanwise structures. The use of Taylor's hypothesis has been demonstrated to be fairly successful in estimating the $\langle\omega_z\rangle$ distributions associated with the large structures (see discussions in Zaman & Hussain 1981). The estimated error for $\langle\omega_z\rangle$ is less than 10%. A pseudo-streamwise coordinate, x^*, defined as

$$\Delta x^* = -U_c \Delta t, \tag{2.2}$$

where Δt is the time delay after the initiation of A/D sampling, is used in the presentation of the results. Defined this way, x^* has units of length but is actually a measure of time. It should not be confused with the actual streamwise distance, x, which does not change when data is acquired at a fixed station of measurement.

One setting of free-stream conditions was used for all experiments conducted in the present study. In the test section of the wind tunnel, the time-mean streamwise velocity on the high-speed side, U_H, was maintained at 5.5 m s^{-1} while that on the low-speed side, U_L, was 1.8 m s^{-1}. The resultant velocity ratio R, defined as $\Delta U/2U_c$where $\Delta U = U_H - U_L$ and $U_c = 0.5(U_H + U_L)$, was 0.51. The boundary layers that emerged from the splitter plate were both laminar. Time-mean measurements performed at $x = 0.64$ cm and $z = 0$ cm showed that the momentum thicknesses were 0.08 cm (θ_H) and 0.15 cm (θ_L) for the high- and low-speed-side boundary layers, respectively. The two-dimensional behaviour of the boundary layers was also examined. Their characteristic scales were measured over the entire span of the splitter plate and the results are

	U_H	U_L	θ_H	θ_L
Uniformity (within)	2%	2%	4%	5%

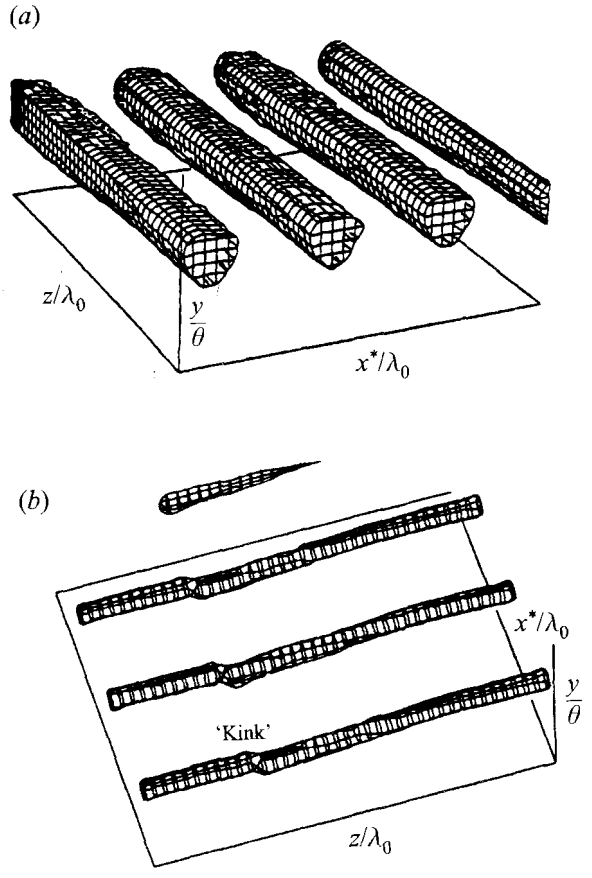

FIGURE 3. Iso-surfaces of ensemble-average spanwise vorticity $\langle\omega_z\rangle$ at the first station (x = 7.62 cm): (*a*) surface value = 0.15 $\langle\omega_z\rangle_{max}$; (*b*) surface value = 0.73 $\langle\omega_z\rangle_{max}$. x^*/λ_0: 0 to +3.0; y/θ: −10.4 to +9.3; z/λ_0: −1.7 to +1.7. θ is the local momentum thickness and λ_0 is the Kelvin–Helmholtz wavelength.

In the remainder of the article, the pseudo-streamwise coordinate, x^*, and the spanwise coordinate, z, are normalized by λ_0; the transverse coordinate, y, is normalized by the local momentum thickness. Ensemble-average vorticity components are normalized by $(\partial U/\partial y)_{max}$ (= 1368 s^{-1}). Some of the normalized $\langle\omega_x\rangle$ and $\langle\omega_z\rangle$ distributions are presented in the form of iso-surface plots. The purpose of showing the plots is to show the existence of any organized three-dimensional fluid motion in the measurement domain. Because of this, the values of the iso-surfaces presented for each station are decided by the ability of the corresponding iso-surfaces to illuminate such motion. As a result, the iso-surfaces presented for different stations may correspond to different values of vorticity.

3. Development of the spanwise rollers

3.1. *Formation of the spanwise structures*

The mixing layer undergoes Kelvin–Helmholtz instability and rolls up into discrete spanwise vortices at the first station. As shown in figure 3(*a*), the spanwise structures are in the form of long cylindrical rollers. They are highly periodic in x^* and

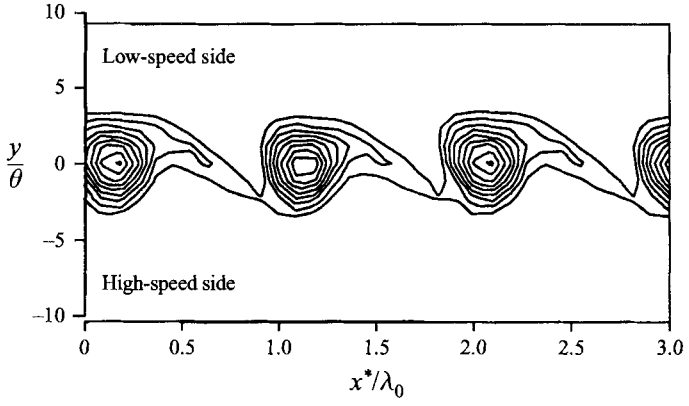

FIGURE 4. Iso-contours of ensemble-average spanwise vorticity $\langle\omega_z\rangle$ in the (x^*, y)-plane $(z/\lambda_0 = 0)$ at the first station (x = 7.62 cm). Contour levels are 0.1 to 0.9 with increment of 0.1. Vorticity values are normalized by $(\partial U/\partial y)_{max} = 1368\ \mathrm{s}^{-1}$.

the average centre-to-centre distance, λ_0, is 2.8 cm (figure 4). This corresponds to a normalized frequency ($= 2\pi\theta_H/\lambda_0$) of 0.18, which matches very well with the most amplified initial instability frequency obtained by Ho & Huang (1982). On iso-surfaces of relatively low $\langle\omega_z\rangle$ values shown in figure 3(*a*), the rollers are nearly straight and parallel to the z-axis. On the other hand, on surfaces corresponding to high vorticity, as shown in figure 3(*b*), a 'kink' exists between $z/\lambda_0 = 0.27$ and 0.36 in the centre of the roller so that the portion of the roller on the $+z$ side is about $0.1\lambda_0$ ahead of (in x^*) the portion on the $-z$ side. Because of this kink, negative streamwise vorticity is generated near the centre of the roller. It will be demonstrated later that the kink evolves into a series of counter-rotating streamwise vortices at the subsequent stations (to be discussed in § 4).

The strength of the rollers is also uniform in the spanwise direction. This is reflected in the circulation about the roller, $\Gamma_z(z)$, which is defined as

$$\Gamma_z(z) = \int_{-\infty}^{+\infty} \int_{x_1^*}^{x_2^*} \langle\omega_z\rangle \mathrm{d}x^* \mathrm{d}y \tag{3.1}$$

where $(x_2^* - x_1^*)$ covers the length of $1.0\lambda_0$ in x^* with the centre of the roller in the middle of the range. When normalized by $(\partial U/\partial y)_{max}(\theta_H + \theta_L)\lambda_0$, the spanwise-average value of Γ_z at the first station is 1.15 and the standard deviation of the distribution is only about 1.5% of the mean value.

3.2. *Pairing of the spanwise structures*

Merging of the spanwise structures begins at the second station and continues through the third and fourth stations. At the second station (figures 5*a* and 6*a*), the spanwise structures assume a staggered pairing formation with one half of the rollers shifted to the high-speed side (the high-speed rollers, HR) and the other half to the low-speed side (the low-speed rollers, LR). At the third station (figures 5*b* and 6*b*), the pairing structures rotate around each other to form discrete T-shaped iso-surfaces in which the LR are on top of the HR. Ho & Huang (1982) designates the location where such behaviour takes place as the pairing location. From the first to the third stations, owing to the roll-up and pairing spanwise vorticity is transported out of the braid region. At the fourth station, this trend is reversed. By this time, the spanwise structures have rotated over $\pi/2$ radians (figures 5*c* and 6*c*) around each

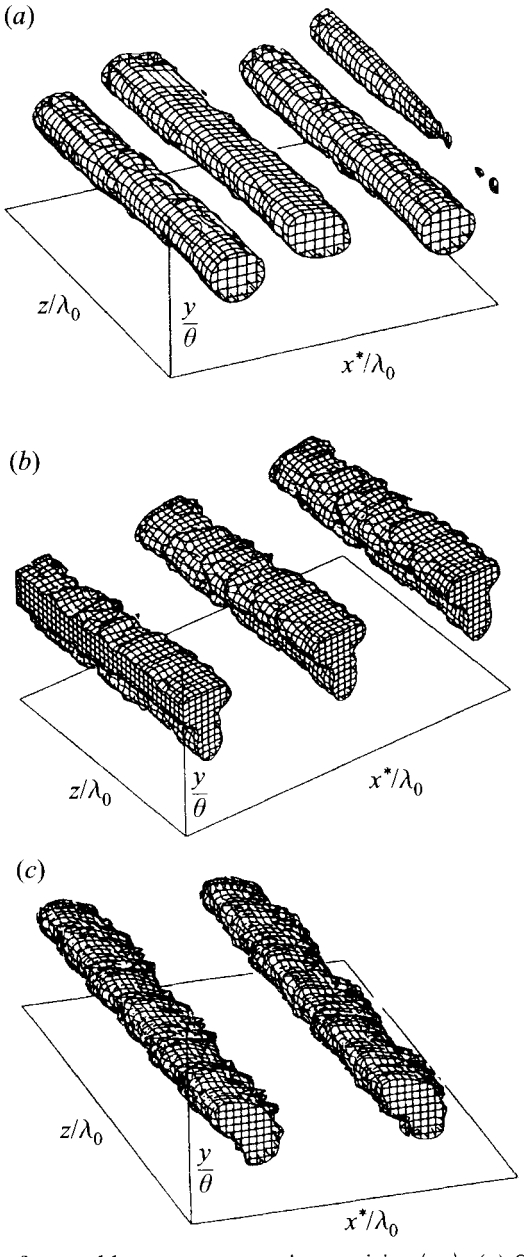

FIGURE 5. Iso-surfaces of ensemble-average spanwise vorticity $\langle\omega_z\rangle$. (*a*) Second station (x = 15.24 cm), surface value = $0.15\langle\omega_z\rangle_{max}$. x^*/λ_0: 0 to +3.1; y/θ: −10.3 to +9.2; z/λ_0: −1.7 to +1.7. (*b*) Third station (x = 22.86 cm), surface value = $0.16\langle\omega_z\rangle_{max}$. x^*/λ_0: 0 to +4.8; y/θ: −6.8 to +6.4; z/λ_0: −1.7 to +1.7. (*c*) Fourth station (x = 26.67 cm), surface value = $0.26\langle\omega_z\rangle_{max}$. x^*/λ_0: 0 to +4.0; y/θ: −4.8 to +9.7; z/λ_0: −3.5 to +3.5.

other. With the structures moving back towards the centreline of the mixing layer, $\langle\omega_z\rangle$ re-enters the vorticity-depleted braid region. Such behaviour, pointed out by Moser & Rogers (1993), allows the three-dimensional activities in the braid region to increase once again after being slowed down by the pairing process (see §4.6 for further discussion).

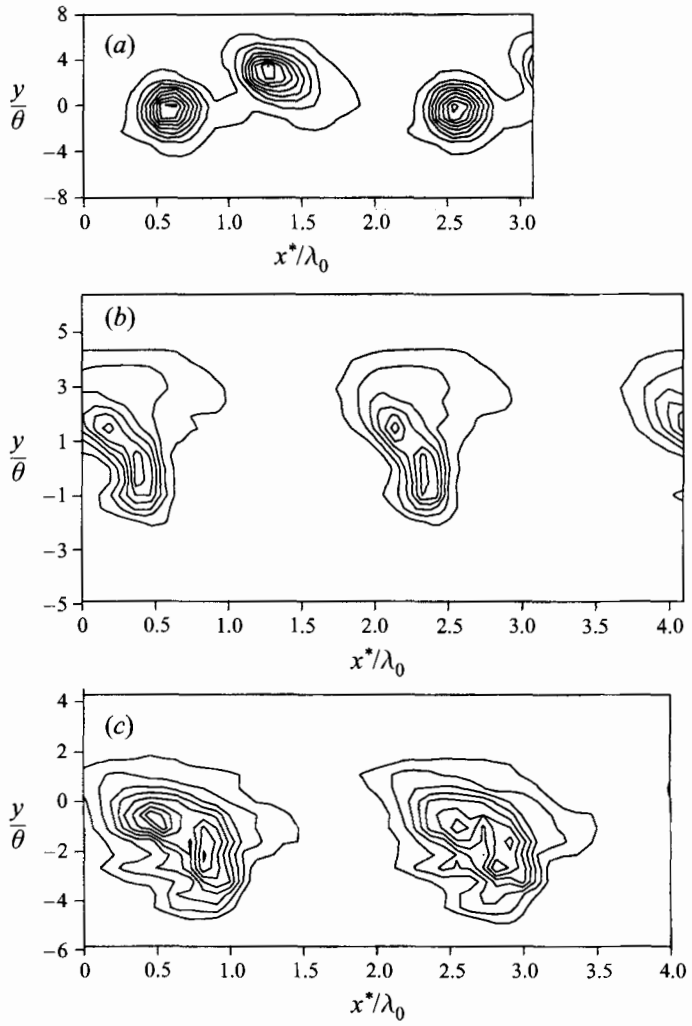

FIGURE 6. Iso-contours of ensemble-average spanwise vorticity $\langle\omega_z\rangle$ in the (x^*, y)-plane $(z/\lambda_0 = 0)$: (*a*) second station (x = 15.24 cm), contour levels are 0.05 to 0.85, increment is 0.1; (*b*) third station (x = 22.86 cm), contour levels are 0.05 to 0.55, increment is 0.1; (*c*) fourth station (x = 26.67 cm), contour levels are 0.05 to 0.4, increment is 0.05. All vorticity values are normalized by $(\partial U/\partial y)_{max} = 1368\ \text{s}^{-1}$.

An examination of the $\langle\omega_z\rangle$ distributions in the centre of the spanwise rollers reveals an increased variability of the location of the roller axes from the single kink at the first station. Figure 7 shows the spanwise variations in x^* locations of peak $\langle\omega_z\rangle$ at different stations. The 'step' in the middle of the profile of the first station is the 'kink' in the spanwise roller discussed earlier in § 3.1. At the second station, the profile of the high-speed roller, HR, consists of one additional kink while the profile of the low-speed roller, LR, has many more kinks and the fluctuation level is higher. At the third and fourth stations, there is a large increase in both the number of kinks and their amplitudes. Statistically, the standard deviations of the profiles in percentages of the initial instability wavelength, λ_0, are: 5% at the first station, 5% for HR at the second station, 7% for LR at the second station, 16% at the third station, and finally 14% at the fourth station. The fluctuations in the profiles, although small, may not

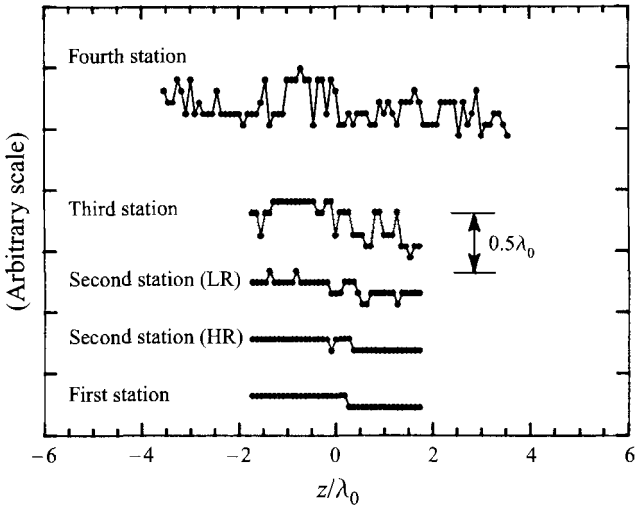

FIGURE 7. Staggered spanwise variations in x^* locations of $\langle\omega_z\rangle_{max}$ (oscillations in the axes of spanwise rollers) at successive streamwise stations.

be totally random. Some features in the profiles, especially those around the region where the first kink is detected, seem to persist from the first to the fourth stations. This suggests that the fluctuations are related to the undulations in spanwise rollers reported by Lasheras & Choi (1988) . Lasheras & Choi did not provide any statistical data on their roller undulations. Based on their flow visualizations pictures alone, it appears that the amplitude of the undulation is slightly higher than the highest fluctuation in the present results. A possible explanation for the difference lies in the nature of the initial conditions: Lasheras & Choi used an indented splitter plate which produced a three-dimensional base flow and a much higher initial perturbation level than the present study. Judging from the iso-surfaces shown in figure 5 for a low-vorticity iso-surface, pairing of the spanwise rollers is extremely periodic and quite two-dimensional. The rollers remain straight but have small fluctuations on the periphery. This suggests a possible increase in Γ_z fluctuation about the spanwise rollers.

Figure 8 shows the staggered profiles of Γ_z at the different stations. Slightly different from the definition provided earlier, the calculation of Γ_z now covers the length of $2.0\lambda_0$ in x^* because of the merging of the spanwise structures. Instead of the centre of the roller, the centre of the roller pair is now in the middle of the range. The results show that the average Γ_z at the second, third, and fourth stations is twice the level at the first station, as expected due to the structures merging. The fluctuation level at the third and fourth stations also doubles the first station's level. However, because the mean Γ_z has also increased, it remains at 1.5% of the mean value, the same as the first station. This result suggests that although the oscillations in the roller axes intensify downstream, they do not result in a major tilting of the spanwise rollers into the streamwise direction. The rollers remain mostly two-dimensional throughout the four stations of measurement.

Although the fluctuation level is low, the spanwise Γ_z profiles contain some interesting features. Among the fluctuations, the more prominent peaks and valleys occur at approximately the same spanwise locations at all three stations. This is particularly true for the valley located just to the positive side of $z = 0$. A comparison between

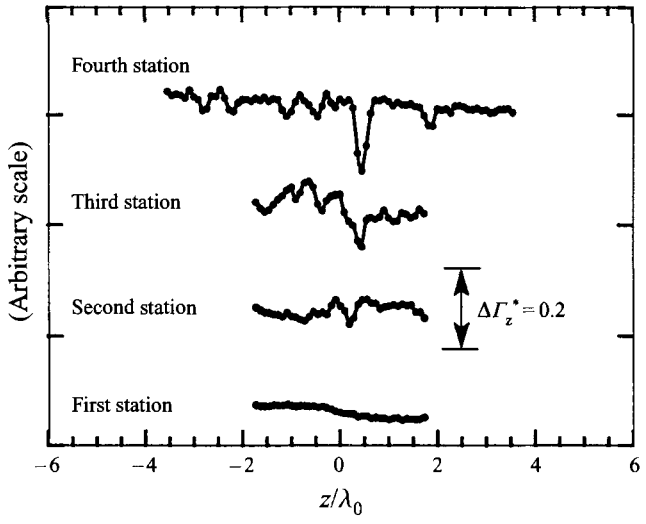

FIGURE 8. Staggered spanwise distributions of the spanwise circulation of the spanwise rollers, Γ_z, at successive streamwise stations. $\Gamma_z^* = \Gamma_z/\Gamma_{z,0}$ where $\Gamma_{z,0} = 0.1$ m^{2}s^{-1} is the spanwise circulation of the spanwise rollers at the first station ($x = 7.62$ cm).

figures 7 and 8 provides some insight into the nature of the valley. The position of the valley matches well with that of the kink in the roller axis at the first station. This suggests that the turning of the spanwise vortex line into the streamwise direction at the kink results in a local depletion of $\langle\omega_z\rangle$ and thus a reduction in Γ_z. Downstream, more kinks develop and Γ_z at the spanwise location of the original kink continues to decrease. This indicates that a mechanism has developed at the original kink spanwise location that continuously channels the spanwise vorticity into a different direction. An example of such a mechanism is a pair of counter-rotating streamwise vortices.

4. Development of the streamwise structures

4.1. *Streamwise vorticity in the initial region*

Normalized $\langle\omega_x\rangle$ at the first station of measurement varies within ± 0.07 in the core region and ± 0.05 in the braid region. Compared to the spanwise vorticity distribution, the peak $\langle\omega_x\rangle$ is about 7% of the peak $\langle\omega_z\rangle$ at this station. This is four times lower than the 30% reported by Huang & Ho (1990) and Bell & Mehta (1992) in time-average measurements. As will be shown later, the circulation associated with the peak $\langle\omega_x\rangle$ is in the same range as the amplitude of the three-dimensional perturbation used by Rogers & Moser (1992) in their numerical simulations.

The three-dimensional $\langle\omega_x\rangle$ distribution at the first station displays very little organization. Figure 9(*a*) shows the positive iso-surfaces of $\langle\omega_x\rangle = 0.3\langle\omega_x\rangle_{max}$. Patches of vorticity can be found across the whole measurement domain. An examination of the negative iso-surfaces provides more or less the same information for the negative $\langle\omega_x\rangle$ distribution. A comparison of the $\langle\omega_x\rangle$ iso-surfaces to the $\langle\omega_z\rangle$ distribution shows that the patches are all confined within the mixing layer. However, unlike the $\langle\omega_z\rangle$ distribution that is dominated by the two-dimensional spanwise vortices, the $\langle\omega_x\rangle$ structures are highly irregular in shape, although some of them are fairly periodic in x^*. The $\langle\omega_x\rangle$ iso-contours in the (y,z)-plane (figures 9*b* and 9*c*) indicate that the vorticity patches do not form any clear spanwise-periodic pattern. However,

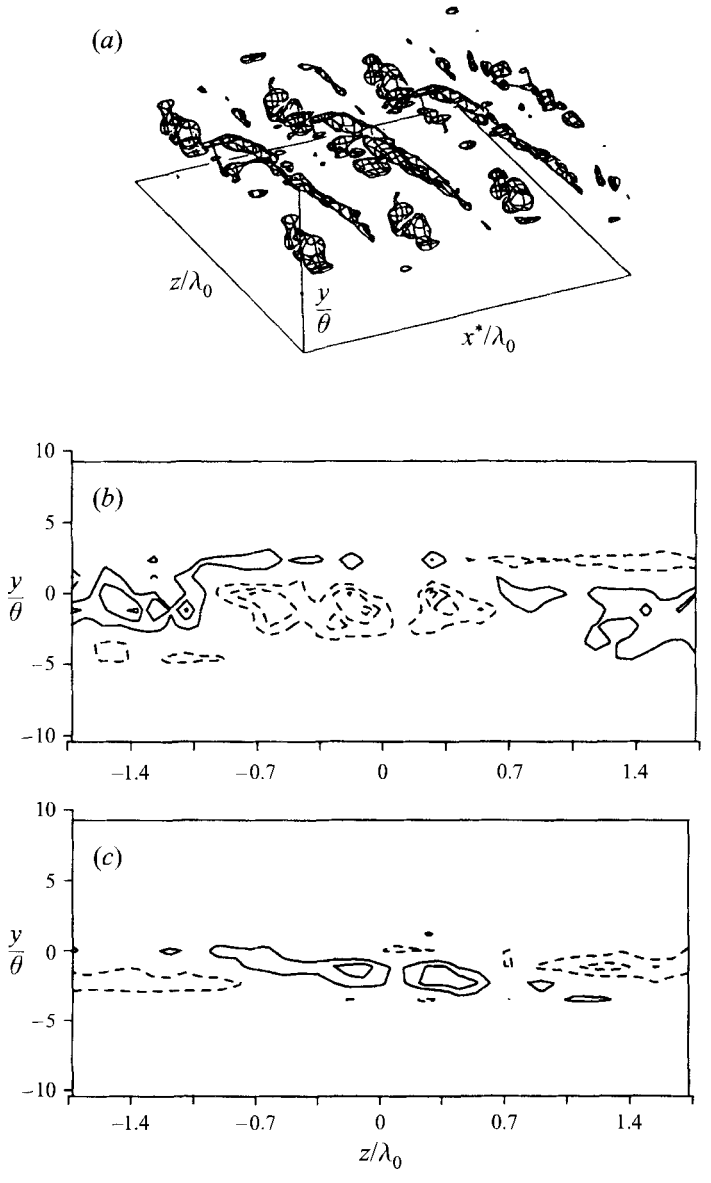

FIGURE 9. Ensemble-average streamwise vorticity, $\langle\omega_x\rangle$, at the first station ($x = 7.62$ cm). (*a*) Positive iso-surfaces, surface value = $0.3\langle\omega_x\rangle_{max}$. x^*/λ_0: 0 to +3.0; y/θ: −10.4 to +9.3; z/λ_0: −1.7 to +1.7. (*b*) Iso-contours in (y,z)-plane in the core region ($x^*/\lambda_0 = 1.2$), contour levels are −0.06 to +0.045, increment is 0.015 and the $\langle\omega_x\rangle = 0$ line is not included. (*c*) Iso-contour in (y,z)-plane in the braid region ($x^*/\lambda_0 = 1.7$), contour levels are −0.06 to +0.045, increment is 0.015 and the $\langle\omega_x\rangle = 0$ line is not included. All vorticity values are normalized by $(\partial U/\partial y)_{max} = 1368\ s^{-1}$.

slightly to the positive side of the z-axis, two $\langle\omega_x\rangle$ peaks can be observed at the same location in both the core and the braid regions. The structures in the core region are more circular than those in the braid region which are flat and elongated in the z-direction. These flat braid structures are similar to the early stage vortices in Rogers & Moser (1992) and Lin & Corcos (1984).

The $\langle\omega_x\rangle$ peaks in the core region have opposite sign to those in the braid region. This behaviour has been predicted by Ashurst & Meiburg (1988) in vortex dynamics

simulations. The explanation for this is that the streamwise vorticity vector at the centre of the spanwise roller rotates as the mixing layer rolls up and is turned 180° from its original orientation when the roll-up is complete. Since the rolling motion in the braid region only tilts the vector without reversing its direction, the $\langle\omega_x\rangle$ in the braid region maintains the same sign as when it is first generated.

The $\langle\omega_x\rangle$ peaks in the core region (figure 9*b*) correspond to the kink in the spanwise roller discussed in § 3.1. The sign of the peaks (negative) is consistent with the $\langle\omega_z\rangle$ results which indicate the spanwise vortex line in the core region turns into the negative x^* direction near $z = 0$. The absence of equal-strength positive peaks next to the observed negative peaks suggests that the kink is not a symmetric horse-shoe-type vortex. This is expected in a natural environment when stationary disturbances may favour the formation of one sign of vorticity over the other. The association of streamwise vortices to stationary upstream disturbances of the mixing layer is further confirmed by the fact that the peaks in the core and braid regions can be found at the same spanwise location. Such behaviour has been previously observed in numerous studies (Bernal & Roshko 1986; Huang & Ho 1990 among others). In the present experimental setup, we back-tracked the footprints of the streamwise structures and discovered that they converged to the location of a very small hole on the surface of the splitter plate at about 20 cm upstream from the trailing edge. Obviously, the mixing layer is very sensitive to localized upstream disturbances, which is probably why streamwise vortices have been observed in many laboratory experiments. However, this is not to say that all streamwise vortices that may develop downstream originate from the same hole. In fact, as will be demonstrated later, there are equally strong streamwise vortices downstream in the mixing layer at other spanwise locations, suggesting the presence of other disturbances.

The results at the first station indicate that stationary streamwise structures exist in the initial roll-up of the mixing layer. However, their $\langle\omega_x\rangle$ levels are low and they do not appear to be strongly periodic in the spanwise direction. Together with the $\langle\omega_z\rangle$ results presented in § 3, it can be concluded that the initial flow field of the present mixing layer is sufficiently two-dimensional. Such a condition is critical for the current study. Without it, it will not be possible to conclude that the development of any strong spanwise mode during the subsequent evolution of the mixing layer is due to an instability mechanism of the mixing layer itself.

4.2. *Initial formation of organized streamwise structures*

The first trace of organized streamwise structures is detected at the second station of measurement. From the iso-surfaces shown in figure 10, three positive longitudinal structures ($\langle\omega_x\rangle > 0$), aligned in the direction of the mean flow, can be identified in the mid-span area. Examination of the negative $\langle\omega_x\rangle$ distribution indicates the existence of negative longitudinal structures side-by-side with the positive ones although they are less well-defined. In the background, patches of isolated vorticity exist. They are similar to those observed at the first station but appear to be more periodic in both x^* and z. A more detailed picture of the longitudinal vortices can be obtained from the iso-contours in the (x^*, y)-plane shown in figure 11. Also included in the figure are the corresponding iso-contours of $\langle\omega_z\rangle$. The (x^*, y)-plane chosen slices through the middle of a negative longitudinal structure. It shows that the $\langle\omega_x\rangle$ distribution associated with the structure is quite different at different x^*. As pointed out in § 3.2, the spanwise structures begin to pair at the second station. The re-orientation of the spanwise rollers creates two distinct braid regions: a shrinking one between two pairing spanwise structures (the shrinking braid or SB) and a widening one between

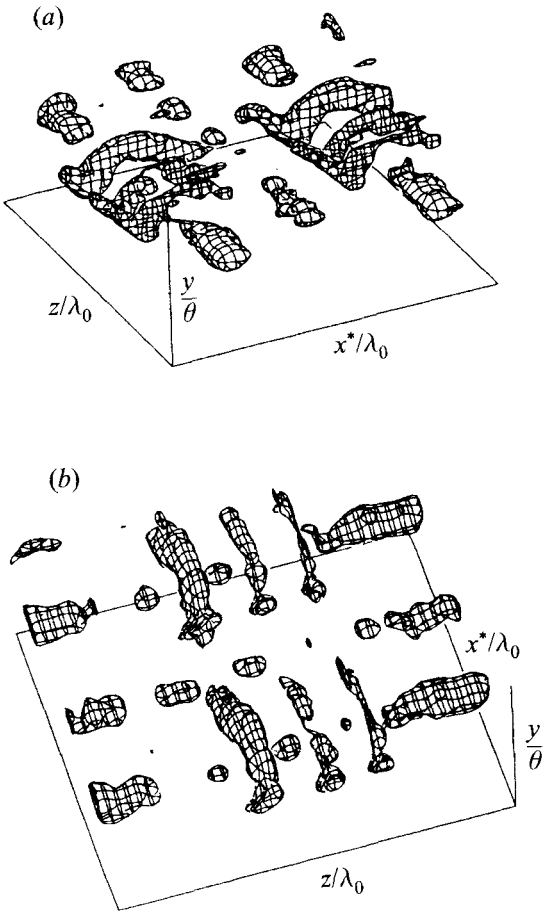

FIGURE 10. Iso-surfaces of ensemble-average streamwise vorticity, $\langle\omega_x\rangle$, at the second station (x = 15.24 cm). Surface value = $0.3\langle\omega_x\rangle_{max}$. x^*/λ_0: 0 to +3.1; y/θ: −10.3 to +9.2; z/λ_0: −1.7 to +1.7. (*a*) The side view; (*b*) the top view.

two spanwise structure pairs (the widening braid or WB). The streamwise structures in the SB rotate with the spanwise structures while being sheared in the mixing-layer-like flow between the pairing structures. The structures in the WB, on the other hand, do not rotate as much but are also stretched continuously due to the widening of the WB. Prominent streamwise structures are found in both regions at the second station. In the SB, the structure extends from the upper periphery of the high-speed roller, HR, to the lower periphery of the low-speed roller, LR. The formation of these structures in the braid region have been visualized in laboratory experiments (Bernal & Roshko 1986; Lasheras *et al.* 1986) and computed in numerical simulations (Metcalfe *et al.* 1987; Rogers & Moser 1992). Hussain (1983, 1986) termed them the 'rib' vortices and pointed out that the region where the rib vortices join the spanwise structures is the source of three-dimensional mixing. This speculation is supported by the present results. As shown in figure 11(*a*), the peak $\langle\omega_x\rangle$ of the rib vortex, an indicator of three-dimensionality, does indeed occur at the connecting points of the streamwise and spanwise vortices. In the WB, similar rib vortices develop. They have approximately the same peak $\langle\omega_x\rangle$ level as those in the SB (about 0.08) but their orientations are different. While the vortices in SB follow the rotation of the pairing

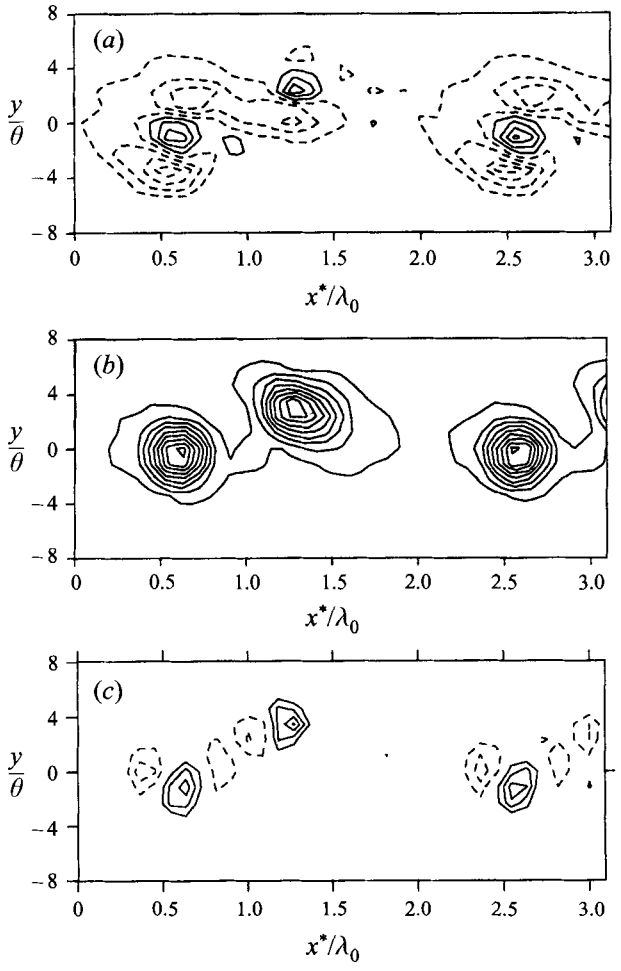

FIGURE 11. Iso-contours of ensemble-average vorticity in the (x^*, y)-plane at the second station (x = 15.24 cm). (*a*) The streamwise component, $\langle\omega_x\rangle$. Contour levels are −0.18 to +0.14, increment is 0.04. (*b*) The spanwise component, $\langle\omega_z\rangle$. Contour levels are 0.05 to 0.85, increment is 0.1. (*c*) The $\langle\omega_z\rangle$ fluctuation, $\langle\omega_z\rangle_f$. Contour levels are −0.12 to +0.16, increment is 0.04. The $\langle\omega_z\rangle_f = 0$ line is not included. All vorticity values are normalized by $(\partial U/\partial y)_{max} = 1368\ \text{s}^{-1}$.

spanwise structures and are almost lined up with the mean flow, those in the WB are aligned with the principle direction of the strain rate.

4.3. *Nature of the three-dimensional instability*

The origin of three-dimensionality or the cause for the formation of organized $\langle\omega_x\rangle$ has been discussed in virtually every recent study of mixing layers. It is generally agreed that the organized streamwise structures are formed through a three-dimensional instability of the mixing layer after the roll-up of the spanwise structures. As for the nature of mechanism involved, there are two theories. Pierrehumbert & Widnall (1982) identified a 'core' instability as the main mechanism. Their results were supported by the instability study performed by Corcos & Lin (1984). A second type of instability, the 'braid' instability, is suggested by other researchers. This is supported by the flow visualizations of streamwise vortices by Lasheras & Choi (1988) and quantitative measurements by Bell & Mehta (1992). Recently, Rogers & Moser (1992) pointed

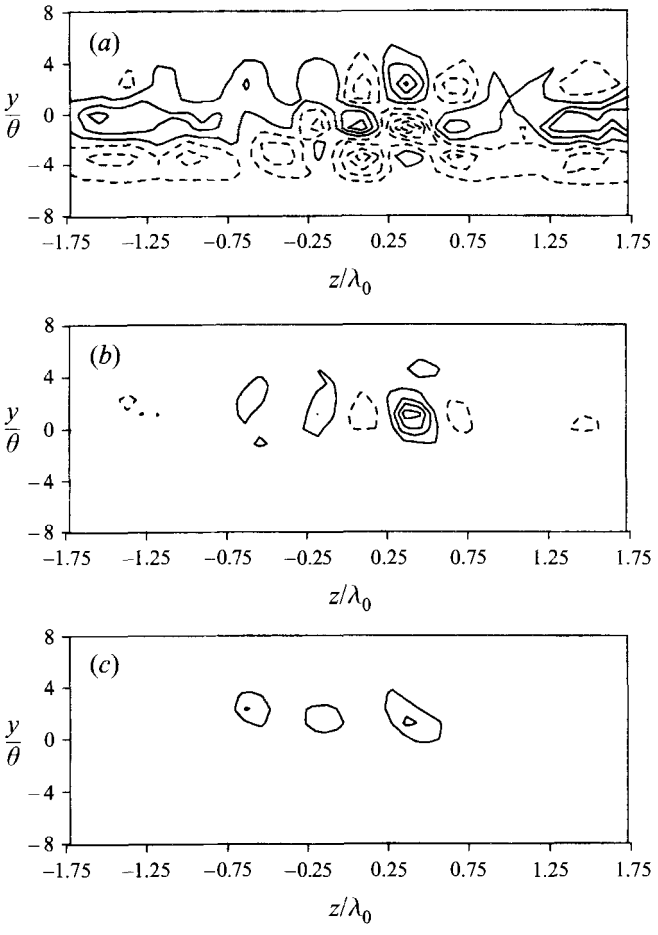

FIGURE 12. Iso-contours of ensemble-average streamwise vorticity, $\langle\omega_x\rangle$, in the (y,z)-plane at the second station (x = 15.24 cm): (*a*) in the core region ($x^*/\lambda_0 = 0.5$), contour levels are −0.22 to +0.14, increment is 0.04; (*b*) in the shrinking braid region, SB ($x^*/\lambda_0 = 0.9$), contour levels are −0.08 to +0.16, increment is 0.04; (*c*) in the widening braid region, WB ($x^*/\lambda_0 = 1.9$), contour levels are −0.04 to +0.08, increment is 0.04. The $\langle\omega_x\rangle = 0$ lines are not included in the contour plots. All vorticity values are normalized by $(\partial U/\partial y)_{max} = 1368\ \text{s}^{-1}$.

out that the three-dimensionality instability actually involves both mechanisms and the whole process should therefore be considered as a global instability of the entire flow.

In the core region, numerical results by Rogers & Moser (1992) show the presence of streamwise vorticity in the centre of the spanwise rollers which is of opposite sign to the streamwise vortices on the periphery of the rollers. Similar formation has been identified in the present study at the second station. As shown in figure 12(*a*), in the (y,z)-plane that slices through the middle of the HR, a cluster of $\langle\omega_x\rangle$ peaks can be found between $z/\lambda_0 = -0.09$ and +0.82. Together, they form three layers of alternating-sign structures whose cross-sections are much more round than the flat structures at the first station. A comparison of these structures to the $\langle\omega_z\rangle$ distribution in the same plane indicates that the top and bottom layers are on the periphery of the spanwise roller while the middle layer is in the centre. The structures on the periphery are sections of the rib vortices previously discussed in § 4.2. The structures

in the centre are the result of the oscillations in roller axis described in § 3.2. In the transverse direction, the layered vortices also alternate in sign so that the structures on the periphery of the roller always have different sign to the corresponding vortex in the centre. This suggests that oscillation of the roller axis is π radians out of phase with the vortex line formed by the rib vortices. A similar configuration in vortex lines has also been computed by Ashurst & Meiburg (1988) and observed by Lasheras & Choi (1988). The spanwise range in which the second station $\langle\omega_x\rangle$ peaks are located corresponds very well to the location of the 'kink' at the first station (see § 4.1), strongly suggesting that the $\langle\omega_x\rangle$ peaks evolve from a 'kink' in the spanwise vortex line. At the first station, the double $\langle\omega_x\rangle$ peaks in the roller centre consist of only negative vorticity. At the second station, these kink-induced peaks have developed into counter-rotating vortices. Similar development was observed by Lasheras *et al.* (1986) where streamwise vortices initiated by a single localized source grew into a series of alternating-sign structures in the spanwise direction. Since the lateral spreading of streamwise vorticity takes place in the spanwise rollers, the mechanism involved should be related to the 'translative instability' described by Pierrehumbert & Widnall (1982).

The three layers of streamwise structures are nearly identical to the 'quadrupoles' of streamwise vorticity described by Rogers & Moser (1992) (their figure 7*b*). According to them, these $\langle\omega_x\rangle$ 'quadrupoles' strengthen $\langle\omega_z\rangle$ on one side of the spanwise rollers while weakening it on the other side. The extent of this distortion can be estimated by examining the distribution of the $\langle\omega_z\rangle$ fluctuation, $\langle\omega_z\rangle_f$, on the (x^*, y)-plane between a pair of counter-rotating streamwise vortices. The quantity $\langle\omega_z\rangle_f$, defined as

$$\langle\omega_z\rangle_f = \langle\omega_z\rangle - \frac{1}{z_2 - z_1}\int_{z_1}^{z_2}\langle\omega_z\rangle \mathrm{d}z, \tag{4.1}$$

is a measure of local $\langle\omega_z\rangle$ deviation from the two-dimensional $\langle\omega_z\rangle$ distributions associated with the spanwise rollers (HR in this case); z_1 and z_2 correspond to the two ends of the spanwise roller under consideration. The iso-contours of $\langle\omega_z\rangle_f$ in figure 11(*c*) clearly show two $\langle\omega_z\rangle_f$ peaks, one negative and one positive, surrounding the centre of the HR. The normalized peak $\langle\omega_z\rangle_f$ level is 0.16 which is about 18% of the local peak $\langle\omega_z\rangle$ value. Similar peaks can also be found attached to the LR.

The strength and organization of the rib vortices are different in the two braid regions, SB and WB. As shown in figures 12(*b*) and 12(*c*), both the SB and WB consist of one row of rib vortices. However, in the SB (figure 12*b*), the vortices are counter-rotating with a normalized peak $\langle\omega_x\rangle$ level of 0.18 while the vortices in the WB are predominantly positive and the peak $\langle\omega_x\rangle$ level is only one half of the level in the SB. The counter-rotating vortices in the SB are apparently the product of intense three-dimensional instability which includes Lin & Corcos's (1984) vortex collapsing (the structures are round) and Lasheras *et al.*'s (1986) lateral propagation of streamwise vorticity (the structures alternate in sign). The structures in the WB, on the other hand, may have collapsed just like the SB structures, but they lack the characteristics of lateral propagation. The fact that their orientation is consistent with the positive $\langle\omega_x\rangle$ peaks in the braid region at the first station suggests that they are the stretched version of the braid structures from the first station. One possibility for their failure in spreading laterally is the depletion of spanwise vorticity in the braid region at the second station. Without it, Lasheras *et al.*'s (1986) type braid instability should not develop.

Clearly, if the SB is considered as part of the core region, the results presented

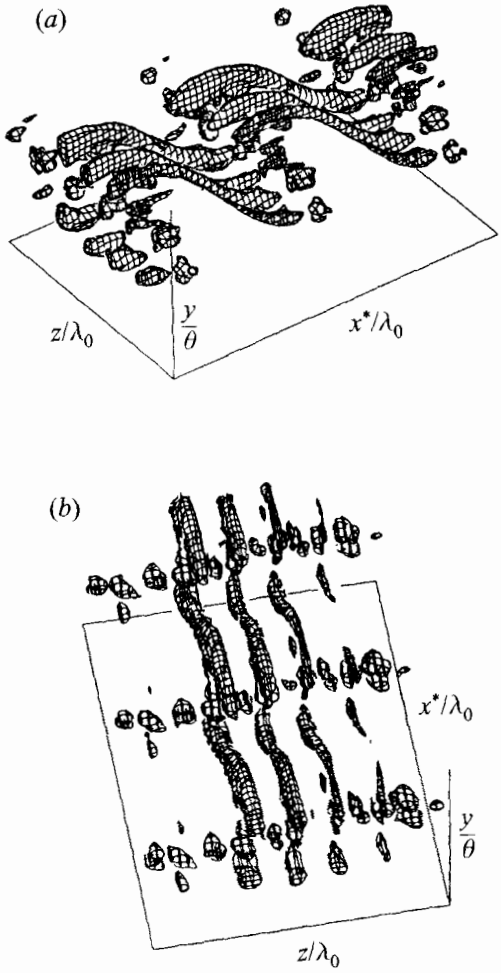

FIGURE 13. Iso-surfaces of the ensemble-average streamwise vorticity, $\langle\omega_x\rangle$, at the third station (x = 22.86 cm). Surface value = $0.2\langle\omega_x\rangle_{max}$. x^*/λ_0: 0 to +4.8; y/θ: −6.8 to +6.4; z/λ_0: −1.7 to +1.7. (*a*) the side view; (*b*) the top view.

above indicate that three-dimensional instability of the mixing layer, at least when it begins, is more active in the core than in the braid region. Although the growth of the braid structures overtakes that of the core structures towards the end of the first spanwise structure pairing (see § 4.6), the role of the core region in the initial stage of three-dimensional instability is much more important than that of the braid region.

4.4. *Development of the streamwise vortices*

Well-defined rib vortices develop in the WB at the third station of measurement. The iso-surface plot at this station (figure 13) indicates the presence of three distinct positive longitudinal vortices whose spanwise location suggests that they originate from the streamwise vortices observed at the second and therefore the first stations. A comparison with the spanwise roller configuration at this station (figure 5*b*) shows that the streamwise structures in the braid regions originate from the upper (low-speed) periphery of a roller pair, extend through the widening braid region, and disappear into the lower (high-speed) periphery of the pair in front. In addition to

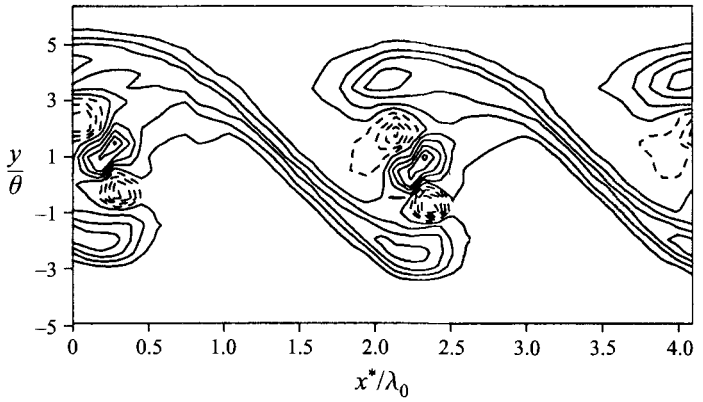

FIGURE 14. Iso-contours of phase-average streamwise vorticity, $\langle\omega_x\rangle$, in the (x^*, y)-plane at the third station (x = 22.86 cm). The plane chosen, $z/\lambda_0 = 0$, slices through the centre of a positive rib vortex. The contour levels are −0.18 to +0.22 and the increment is 0.04. All vorticity values are normalized by $(\partial U/\partial y)_{max} = 1368\ \mathrm{s}^{-1}$.

the longitudinal structures, figure 13 also shows small $\langle\omega_x\rangle$ volumes in the core region which, at this station, consist of pairing spanwise rollers. The details of the $\langle\omega_x\rangle$ volumes are illuminated by the $\langle\omega_x\rangle$ iso-contours in a (x^*, y)-plane that cuts through one of the positive rib vortices as shown in figure 14. A complex but periodic flow pattern exists in the core region. Clearly visible around the periphery of the spanwise structure pairs are part of the longitudinal rib vortices that dominate the iso-surface diagrams in figure 13. Within the core region, three counter-rotating streamwise vortices form a line that is slightly tilted towards the left. The negative structure on the top (low-speed side) is at the centre of the LR while the one on the bottom (high-speed side) is at the centre of the HR. Trapped in between them is the positive structure which is apparently the remnant of the rib vortex in the shrinking braid, SB, observed at the second station. It rotates with the pairing rollers while being constantly strained in the mixing layer formed in the region between the rollers. The peak $\langle\omega_x\rangle$ level of the positive structure is about 25% higher than that of the rib vortex. This is another indication that three-dimensional activities are more intense in the core than in the braid. The stacked vorticity pattern has been previously observed by both Corcos & Lin (1984) and Moser & Rogers (1993) (their figure 9) in computational studies. As pointed out by Moser & Rogers (1993), the complex $\langle\omega_x\rangle$ distribution in the core region is a result of a linear evolution of the mixing layer in which the shearing and turning of the streamwise vortices are accumulative. In other words, the whole process will repeat itself if further pairing of the spanwise rollers takes place.

Topological models proposed by Bernal & Roshko (1986) and Lasheras & Choi (1988) for the rib vortices both consist of a continuous vortex line that loops back and forth between adjacent spanwise rollers forming counter-rotating streamwise vortex pairs and hairpin-like configurations on the periphery of the rollers. Such a model is confirmed by the present results. Figure 15 displays the iso-contours of $\langle\omega_x\rangle$ and $\langle\omega_z\rangle$ in a (y, z)-plane that slices through the edge of a roller pair at the third station (see figure 14). The $\langle\omega_x\rangle$ iso-contours show a single row of counter-rotating peaks on the low-speed side of the core region and the $\langle\omega_z\rangle$ iso-contours consist of a matching row of same-sign peaks. A comparison between figures 15(*a*) and 12(*b*) indicates that the $\langle\omega_z\rangle$ peaks occur between the positive and negative peaks of alternating counter-

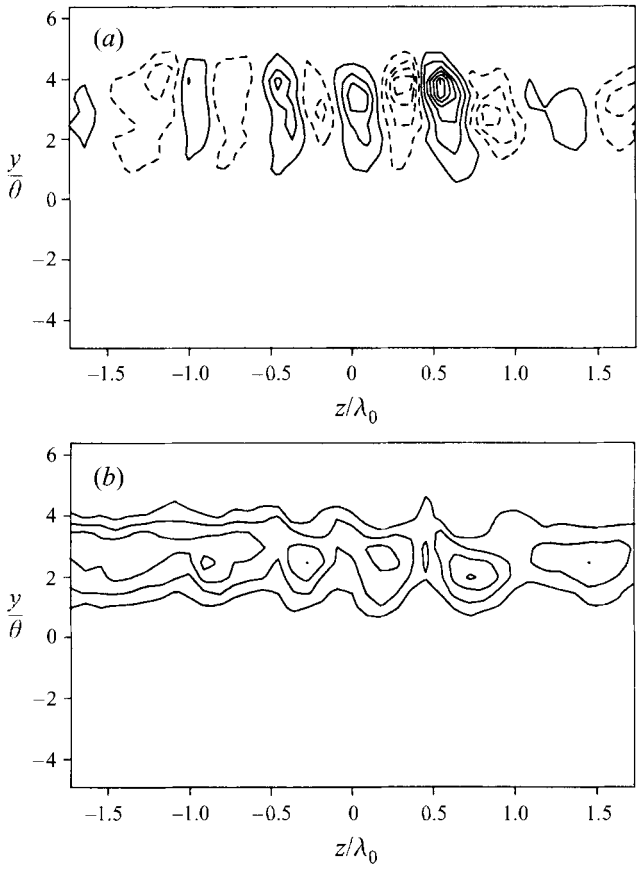

FIGURE 15. Iso-contours of phase-average vorticity in the (y,z)-plane in the core region ($x^*/\lambda_0 = 2.7$) at the third station ($x = 22.86$ cm). (*a*) The streamwise component, $\langle\omega_x\rangle$. Contour levels are −0.18 to +0.26, increment is 0.04. (*b*) The spanwise component, $\langle\omega_z\rangle$. Contour levels are 0.04 to 0.16, increment is 0.04. All vorticity values are normalized by $(\partial U/\partial y)_{max} = 1368\ \mathrm{s}^{-1}$.

rotating $\langle\omega_x\rangle$ pairs. This result is consistent with the configuration of a vortex line initially in the $-x^*$ direction making a U-turn and continuing on in the opposite direction.

The more prominent rib vortices observed at the second and third stations mostly appear around $z = 0$. To investigate the possible existence of vortices at other spanwise locations, the spanwise extent of measurement at the fourth station was doubled. Figure 16 displays a very revealing three-dimensional view of the $\langle\omega_x\rangle$ distribution at this station. In addition to those structures at $z = 0$, rib vortices of similar strength (based on the thickness of structures as a rough measure) exist at other spanwise locations (e.g. close to the origin). This suggests that the small hole on the splitter plate discussed in §4.1 is not the only triggering source of streamwise vortices. Disturbances, large and small, at different upstream locations initiate the formation of additional but different strength vortices. Together, the vortices grow and re-align themselves downstream so that the more dominant vortices become localized at fixed spanwise locations. In other words, removing the hole at $z = 0$ will not remove all the rib vortices in the mixing layer but will probably change the locations of the strong vortices. This behaviour has been observed by Bernal & Roshko (1986)

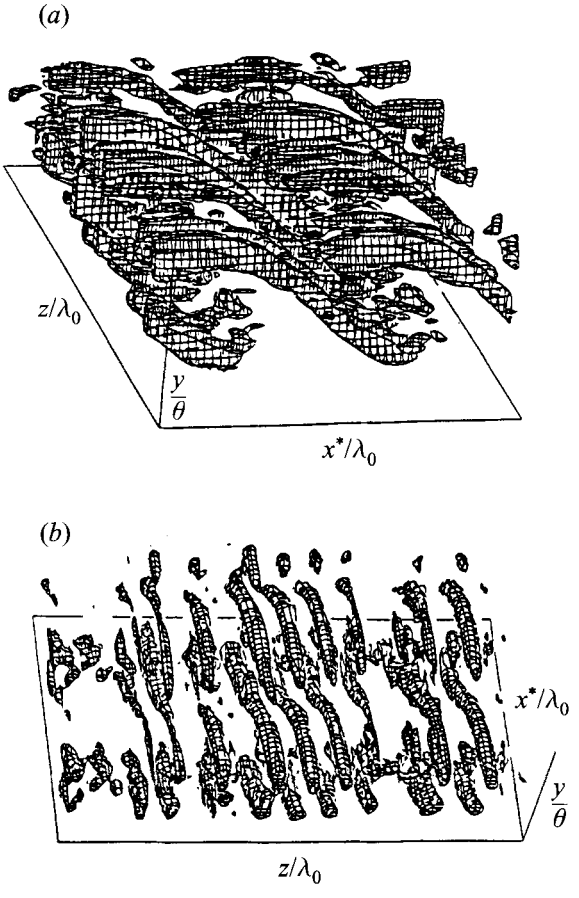

FIGURE 16. Iso-surfaces of ensemble-average streamwise vorticity, $\langle\omega_x\rangle$, at the fourth station (x = 26.67 cm). Surface value = $0.1\langle\omega_x\rangle_{max}$. x^*/λ_0: 0 to +4.0; y/θ: −4.8 to +9.7; z/λ_0: −3.5 to +3.5. (*a*) The side view; (*b*) the top view.

in flow visualizations when changing the screens in the settling chamber of the water tunnel resulted in changes in the positions of the streaky structures which marked the presence of dominant streamwise vortices.

4.5. *Spanwise vortex spacing of the streamwise structures*

The $\langle\omega_x\rangle$ distributions at the four stations of measurement suggest that the streamwise structures are the result of a global spanwise instability of the mixing layer. To obtain a quantitative measure of the stability mechanism, the average spanwise spacing between the streamwise vortices at different stations is measured. Except for the first station where no regular spanwise pattern in $\langle\omega_x\rangle$ is observed, the spacing at each station is determined by measuring the average spanwise distance between the centres of two counter-rotating streamwise vortices that appear at approximately the same y-level in the $\langle\omega_x\rangle$ iso-contours of the (y,z)-plane. The (y,z)-plane that cuts through the core region is usually chosen for the measurement because the vortices in this plane are better defined than those in the braid region, as previously demonstrated. Since the number of recognizable streamwise vortices is different at different stations, the number of vortices over which the average spacing is calculated is also different.

In stability experiments, Lasheras & Choi (1988) and Nygaard & Glezer (1991)

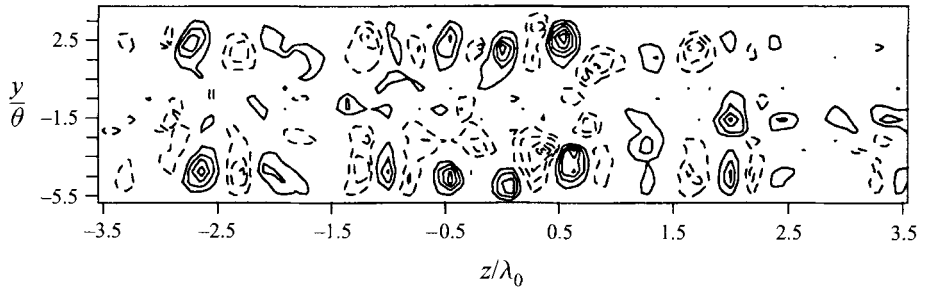

FIGURE 17. Iso-contours of phase-average streamwise vorticity, $\langle\omega_x\rangle$, in the (y,z)-plane in the core region ($x^*/\lambda_0 = 2.5$) at the fourth station ($x = 26.67$ cm). Contour levels are -0.24 to $+0.04$, increment is 0.04. The $\langle\omega_x\rangle = 0$ line is not included. All vorticity values are normalized by $(\partial U/\partial y)_{max} = 1368\ \text{s}^{-1}$.

have reported no significant difference in the growth rate of different spanwise wavelengths. The regularity in spanwise spacing of the present streamwise vortices indicates that there is, however, a preferred wavelength in a naturally developed flow. The normalized average spanwise spacing, s_z(= spacing/λ_0), at the second and third stations is 0.3. At the fourth station, a measurement based on the vortices in the $z = 0$ area is 0.3. Around $z = -1.7$, what appears to be localized merging of the streamwise structures renders s_z to be 0.6 at that particular location. If the s_z obtained this way is considered as one half of the most amplified spanwise wavelength (because the spacing between counter-rotating instead of identical-sign vortices is measured), the ratio of the spanwise to the streamwise wavelength is initially 0.6 and becomes a mix of 0.6 and 1.2 downstream. The first number matches closely with the 2/3 ratio predicted by Pierrehumbert & Widnall (1982) for the most amplified spanwise/streamwise wavelength of a translative core instability. It is also within range of the direct measurements by Bell & Mehta (1992) although their time-average results suffer from the fact that the sign and level of $\langle\omega_x\rangle$ change significantly with time, as indicated by the phase-average results. The doubling of the streamwise vortex spacing at the fourth station (toward the end of spanwise structure merging) has been previously predicted by Bernal & Roshko (1986) and Huang & Ho (1990). This behaviour does not take place uniformly across the entire span because the streamwise structures merge only at isolated locations. The $\langle\omega_x\rangle$ iso-contours at the fourth station indicate the structures departing from row-formation established in the earlier stations and move into a more random distribution (figure 17). Similar re-distributions of the $\langle\omega_x\rangle$ peaks have also been observed by Rogers & Moser (1993) (see their figure 6). According to them, a doubling in s_z occurs only after three or more pairings of the spanwise rollers in a slightly-perturbed flow, instead of at the end of the first merging.

As discussed in § 3.2, except for low-amplitude oscillations in their axes, large-scale undulations never develop in the spanwise rollers. The acoustic forcing applied to the mixing layer certainly suppresses this type of three-dimensional motion but the development of relatively strong rib vortices should have induced a much larger distortion in the rollers than what was observed. An explanation for this may have been offered by Nygaard & Glezer (1991) who found that undulations in the spanwise vortices developed only if the spanwise wavelength associated with the streamwise vortices exceeded λ_0. This is not the case in the present experiment where the naturally developed spanwise wavelength is predominantly $\frac{2}{3}\lambda_0$. If the speculation by Rogers & Moser (1993) on the doubling of spanwise wavelength is valid, large-scale

roller undulation should not take place within the streamwise range examined by the present study. In fact, it may never happen in the present mixing layer because turbulent transition is likely to prevent further merging of the spanwise rollers.

4.6. *Growth of the streamwise structure intensity*

There are two quantities that can be used to characterize the intensity of streamwise structures at each station of measurement: the peak $\langle\omega_x\rangle$ level and the circulation associated with the peak evaluated in a plane normal to the streamwise direction, Γ_x, defined as

$$\Gamma_x(x) = \int_{z_1}^{z_2}\int_{y_1}^{y_2}\langle\omega_x\rangle \mathrm{d}y\mathrm{d}z. \tag{4.2}$$

When evaluating the double integral in the (y,z)-plane, the surface area covered, $(y_2 - y_1)(z_2 - z_1)$, is chosen so that it includes all the vorticity of the streamwise structure under examination. At the stations where well-defined streamwise vortices develop, $(z_2 - z_1)$ is about $\frac{1}{2}s_z$ while $(y_2 - y_1)$ is slightly larger than $\frac{1}{2}s_z$ because the streamwise structures are usually elliptical in shape with the longer axis in the y-direction.

Three types of $\langle\omega_x\rangle$ peaks are examined: the peak at the centre of the spanwise roller, P_c; the peak in the rib vortex on the periphery of the roller, P_p; and the peak in the braid region between the rollers, P_b. The first two quantities measure the three-dimensional intensity in the core region while the last one measures that in the braid region. Figure 18(*a*) displays the streamwise variation of the positive peaks. In the figure, P_c grows almost linearly from the first to the third stations. This increase is apparently due to the intensification of three-dimensional behaviour in the centre of the rollers, as demonstrated earlier in § 3.2 by the increase in waviness of the roller axes. At the fourth station, P_c drops by 25% from the level at the third station. This is due to the collapse of the layered streamwise vortices discussed in § 4.5. Following the collapse, the ensuing streamwise vorticity re-distribution results in lower phase-coherent vorticity and a smaller peak level. Similar trends can also be observed in the P_p variation except that the level of P_p remains at about 30% higher than that of P_c at all times, suggesting that the interaction between the rib vortices and the periphery of the spanwise roller generates stronger three-dimensional activity than the oscillation of the roller itself. The behaviour of P_b, on the other hand, is quite different. It assumes an exponential growth from the first to the fourth station, similar to what has been observed by Rogers & Moser (1992) during the initial roll-up of the mixing layer. The level of P_b, or the strength of the rib vortices in the braid region, does not decrease from the third to the fourth stations even though the P_c variation indicates a more two-dimensional flow in the core region.

Figure 18(*b*) shows the evolution of Γ_x. Like $\langle\omega_x\rangle$ peaks, the circulation of streamwise vortices in different areas is shown separately. The distributions of Γ_x and $\langle\omega_x\rangle$ peaks are similar, as should be expected. In the core region, both in the centre and on the periphery, Γ_x increases from the first to the third stations and decreases at the fourth station. In the braid region, Γ_x increases from the first through the fourth stations. However, unlike the $\langle\omega_x\rangle$ peak distribution, the growth is not exponential and a plateau seems to exist between the second and the third stations. Such a plateau in Γ_x has been previously predicted by Moser & Rogers (1993) to occur during spanwise structure pairing when the braid region is depleted of spanwise vorticity. According to their results, Γ_x will increase once again as soon as spanwise vorticity re-enters the braid region, which occurs when the pairing spanwise structures

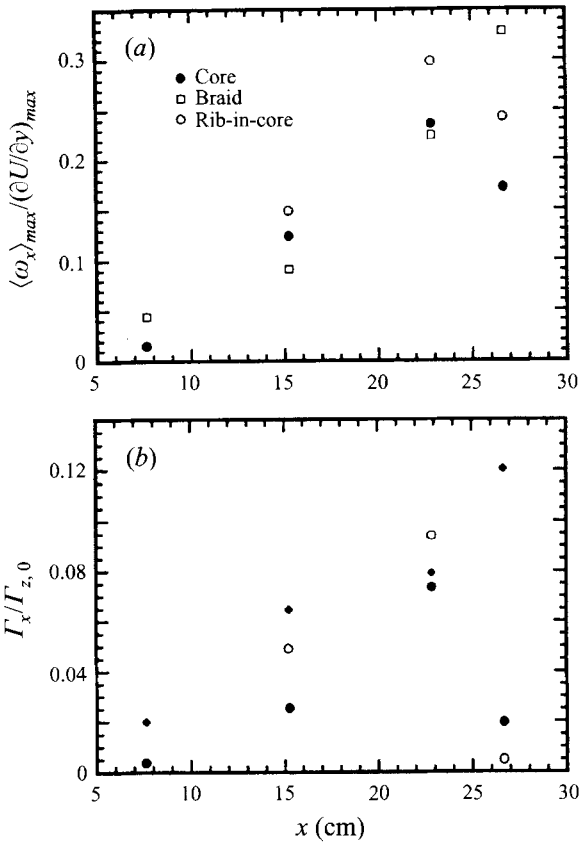

FIGURE 18. Streamwise distribution of (*a*) peak streamwise vorticity, $\langle\omega_x\rangle_{max}$, and (*b*) peak streamwise circulation, Γ_x. $\langle\omega_x\rangle_{max}$ is normalized by $(\partial U/\partial y)_{max} = 1368\ \mathrm{s}^{-1}$ and Γ_x by $\Gamma_{z,0} = 0.1\ \mathrm{m}^2\mathrm{s}^{-1}$, the spanwise circulation of the spanwise rollers at the first station ($x = 7.62$ cm). Core refers to the streamwise structures at the centre of the spanwise rollers, braid to the rib vortices in the braid region, and rib-in-core to the parts of the rib vortices which are on the periphery of the spanwise rollers.

co-rotate past $\pi/2$ radians. Such re-entry of spanwise vorticity, suggested by them, can be demonstrated by the evolution of ω_b, the peak $\langle\omega_z\rangle$ in the braid region. As demonstrated by the $\langle\omega_z\rangle$ iso-contours in § 3.2, a similar pairing sequence also takes place in the present study from the second to the fourth stations. Based on the definition given by Rogers & Moser (1992), ω_b is the maximum $\langle\omega_z\rangle$ in the (y,z)-plane mid-way between the centre of two spanwise structures or structure pairs during pairing. The variation of ω_b, shown in figure 19, indicates that there is indeed a jump in ω_b from the third to the fourth stations after a continuous decrease from the first to the third stations.

5. Development of the mean flow

Growth of the mean flow in the initial region of the mixing layer is governed by the behaviour of the spanwise structures. Figure 20(*a*) shows the growth of θ, defined as

$$\theta = \frac{1}{(\Delta U)^2}\int_{-\infty}^{+\infty}[U_H - U(y)][U(y) - U_L]\mathrm{d}y, \tag{5.1}$$

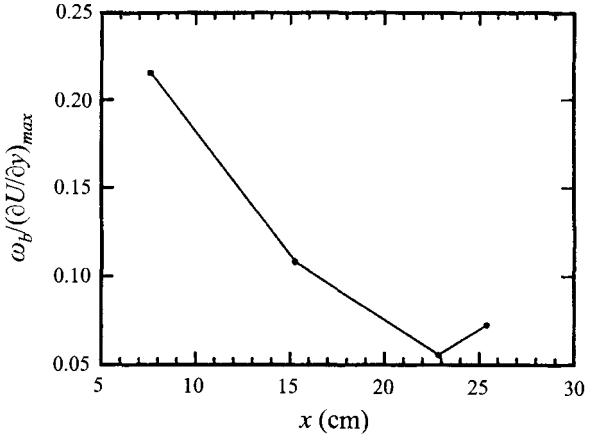

FIGURE 19. Streamwise variation of the peak spanwise vorticity in the braid region, ω_b. The values are normalized by $(\partial U/\partial y)_{max} = 1368\ \mathrm{s}^{-1}$.

in a streamwise range which includes the four stations of measurement. The variation of θ in the forced flow shows typical plateaus where regular roll-up and merging of the spanwise rollers take place (Ho & Huang 1982). Note that without subharmonic forcing, the unforced flow does not have a plateau or, thus, regular merging (at $x \approx$ 25 cm) like the forced flow.

The characteristics of the mean flow are affected by the interactions between the spanwise and streamwise structures, especially when the streamwise structures become stronger as they move downstream. Figure 20(*b*) demonstrates the spanwise distribution of θ at the four stations of measurement. The profiles at the first two stations are fairly flat: the maximum deviation from the mean value is only about 7% of the mean value. Profiles at the next three stations are clearly more wavy: the maximum deviation is 16% at the third station, 22% at the fourth station, and 14% at the fifth station. A comparison between the different profiles also reveals that the more prominent peaks and valleys are aligned in the streamwise direction, similar to the behaviour of the Γ_z distribution shown in § 3.2. This is also in agreement with earlier findings by Jimenez (1983) and Huang & Ho (1990) who observed similar behaviour in the time-average velocity measurements. The variations in θ indicate a x-momentum transfer in the y-direction that takes place unevenly over the span of the mixing layer. This can be demonstrated by a comparison between the θ-profile and the $\langle\omega_x\rangle$ iso-contours at the third station. In figure 21, the peaks and valleys of the θ-profile are highly correlated with the locations of the streamwise vortices in the core region. Specifically, the peaks in the profile are located between pairs of counter-rotating vortices, indicating that the rotation of the vortices transfers high-x-momentum fluid away from the centre of the spanwise structures toward the free stream. Conversely, low-momentum fluid is transported into the centre of the spanwise structures between alternating pairs of counter-rotating streamwise vortices, as indicated by the valleys in the θ-profile at those locations.

6. Concluding remarks

In the present study, three-dimensional vorticity distributions of an acoustically excited mixing layer were computed from measured velocity distributions and the development of natural streamwise vortices was examined. The existence of organized

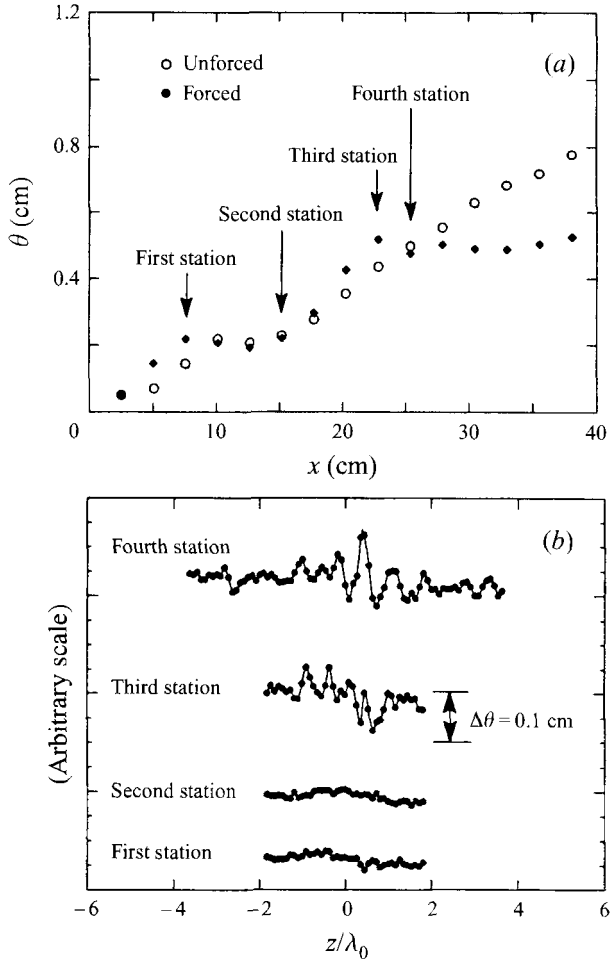

FIGURE 20. (*a*) Streamwise distributions of the momentum thickness, θ, of a forced and an unforced mixing layer. (*b*) Staggered spanwise distributions of the momentum thickness, θ, at successive streamwise stations in a forced mixing layer.

streamwise vortices with a preferred spanwise mode was conclusively demonstrated through three-dimensional $\langle\omega_x\rangle$ distributions. Since no artificial forcing was applied and the boundary layers upstream were two-dimensional, the streamwise vortices must be inherent features of the mixing layer at the Reynolds number investigated.

The results of the three-dimensional flow field were computed from statistically independent time series obtained by a single x-wire probe. The fact that the resultant streamwise vortices were found to be located at fixed spanwise locations indicates that they originate from stationary disturbances in the otherwise two-dimensional spanwise vortex sheet in the initial region. The disturbance first appears as a kink or local change in curvature in the axis of the spanwise structures resulting from the initial roll-up of the mixing layer. Subsequent development of streamwise vorticity from the kink bears many similarities with the results of linear perturbation simulations. In addition to the development of rib vortices which has been predicted by many previous experimental works, the existence of complex but organized streamwise vortices in the core region during the merging of the spanwise rollers has been demonstrated for the first time. Phase-coherent vorticity and circulation associated

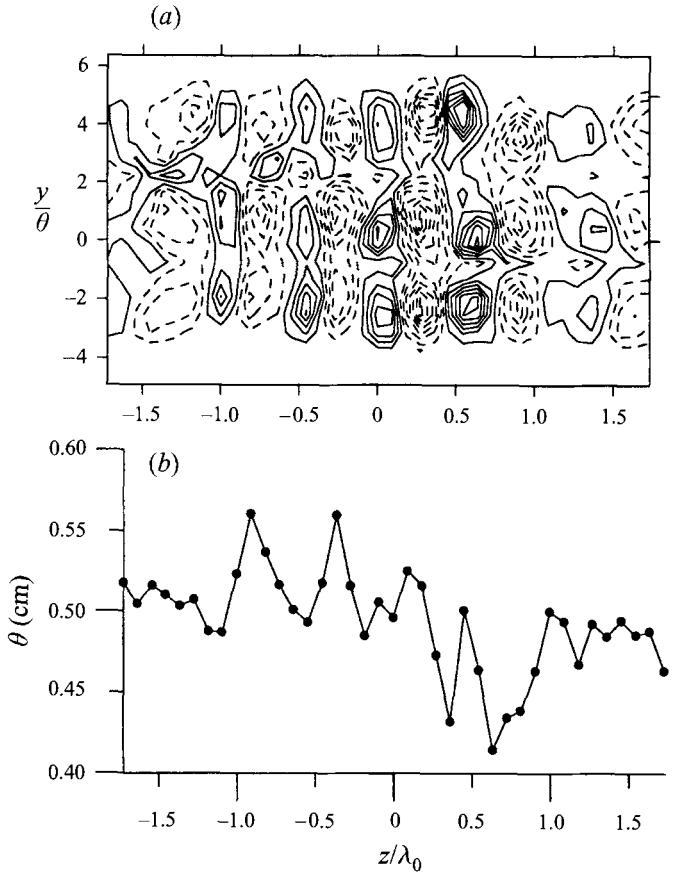

FIGURE 21. Comparison of the streamwise vorticity and momentum thickness distributions at the third station ($x = 22.86$ cm). (*a*) Iso-contours of ensemble-average streamwise vorticity, $\langle\omega_x\rangle$, in the (y,z)-plane in the core region ($x^*/\lambda_0 = 2.3$). Contour levels are -0.3 to $+0.22$, increment is 0.04. All vorticity values are normalized by $(\partial U/\partial y)_{max} = 1368\ \mathrm{s}^{-1}$. (*b*) The spanwise distribution of the momentum thickness, θ.

with the core streamwise structures are more intense than the rib vortices in the braid region except towards the end of the spanwise structure pairing. By this time, instantaneous hot-wire signals indicate that turbulent bursts have emerged in the core region. The exact location where the bursts occur is beyond the scope of the present work, but it can be speculated that the bursts are the result of intense shearing and tearing activities that take place among the core structures. In light of this, the importance of the core instability in the transitional stage of a mixing layer appears to outweigh that of the braid instability, even though the braid structures continue to grow as the mixing layer develops downstream.

Finally, the anticipated doubling in spanwise spacing between the streamwise vortices does not materialize at this high Reynolds number as predicted by previous time-averaged measurements. The present results show that the layered formation of the streamwise vortices which initially consists of a preferred spanwise wavelength collapses at the end of the spanwise structure pairing and no new wavelength emerges. Numerical simulations by Rogers & Moser (1993) have predicted that a change in the spanwise wavelength takes place only after three or more pairings of the spanwise structures. Therefore, it would appear that the ratio of the spanwise to the streamwise

wavelength is only a constant when the streamwise vortices first form. This suggests that the secondary instability of the mixing layer disengages itself from the primary instability (the formation of the spanwise structures) shortly after its initiation stage.

REFERENCES

ASHURST, W. T. & MEIBURG, E. 1988 Three-dimensional shear layers via vortex dynamics. *J. Fluid Mech.* **189**, 87–116.

BELL, J. H. & MEHTA, R. D. 1989 Three-dimensional structure of plane mixing layers. *JIAA Rep. TR*-90. Dept. of Aeronautics and Astronautics, Stanford University.

BELL, J. H. & MEHTA, R. D. 1992 Measurements of the streamwise vortical structures in a plane mixing layer. *J. Fluid Mech.* **239**, 213–248.

BERNAL, L. P. & ROSHKO, A. 1986 Streamwise vortex structure in plane mixing layers. *J. Fluid Mech.* **170**, 499–525.

BREIDENTHAL, R. 1981 Structure in turbulent mixing layers and wakes using a chemical reaction. *J. Fluid Mech.* **109**, 1–24.

CORCOS, G. M. & LIN, S. J. 1984 The mixing layer: deterministic models of a turbulent flow. Part 2. The origin of the three-dimensional motion. *J. Fluid Mech.* **139**, 67–95.

HO, C.-M. & HUANG, L.-S. 1982 Sub harmonic and vortex merging in mixing layers. *J. Fluid Mech.* **119**, 443–473.

HUANG, L.-S. & HO, C.-M. 1990 Small-scale transition in a plane mixing layer. *J. Fluid Mech.* **210**, 475–500.

HUSSAIN, A. K. M. F. 1983 *Turbulence and Chaotic Phenomena in Fluids* (ed. T. Tatsumi), pp. 453–460. North-Holland.

HUSSAIN, A. K. M. F. 1986 Coherent structures and turbulence. *J. Fluid Mech.* **173**, 303–356.

HUSSAIN, A. K. M. F., KLEIS, S. J. & SOKOLOV, M. 1980 A 'turbulent spot' in an axisymmetric free shear layer. Part 2. *J. Fluid Mech.* **98**, 97–135.

JIMENEZ, J. 1983 A spanwise structure in the plane shear layer. *J. Fluid Mech.* **132**, 319–336.

KONRAD, J. H. 1976 An experimental investigation of mixing in two-dimensional turbulent shear flows with applications to diffusion-limited chemical reactions. *Intern. Rep.* CIT-8-PU, Calif. Inst. Technol., Pasadena, CA.

LASHERAS, J. C., CHO, J. S. & MAXWORTHY, T. 1986 On the origin and evolution of streamwise vortical structures in a plane, free shear layer. *J. Fluid Mech.* **172**, 231–258.

LASHERAS, J. C. & CHOI, H. 1988 Three-dimensional instability of a plane free shear layer: an experimental study of the formation and evolution of streamwise vortices. *J. Fluid Mech.* **189**, 53–86.

LIN, S. J. & CORCOS, G. M. 1984 The mixing layer: deterministic models of a turbulent flow. Part 3. The effect of plane strain on the dynamics of streamwise vortices. *J. Fluid Mech.* **141**, 139–178.

METCALFE, R. W., ORSZAG, S. A., BRACHET, M. E., MENON, S. & RILEY, J. J. 1987 Secondary instability of a temporally growing mixing layer. *J. Fluid Mech.* **184**, 207–243.

MOSER, R. D. & ROGERS, M. M. 1993 The three-dimensional evolution of a plane mixing layer: pairing and transition to turbulence. *J. Fluid Mech.* **247**, 275–320.

NYGAARD, K. J. & GLEZER, A. 1991 Evolution of streamwise vortices and generation of small-scale motion in a plane mixing layer. *J. Fluid Mech.* **231**, 257–301.

PIERREHUMBERT, R. T. & WIDNALL, S. E. 1982 The two- and three-dimensional instabilities of a spatially periodic shear layer. *J. Fluid Mech.* **114**, 59–82.

RILEY, J. J. & METCALFE, R. W. 1980 Direct numerical simulations of a perturbed, turbulent mixing layer. *AIAA Paper* 80–0274.

ROGERS, M. M. & MOSER, R. D. 1992 The three-dimensional evolution of a plane mixing layer: the Kelvin-Helmholtz rollup. *J. Fluid Mech.* **243**, 183–226.

ROGERS, M. M. & MOSER, R. D. 1993 Spanwise scale selection in plane mixing layers. *J. Fluid Mech.* **247**, 321–337.

ZAMAN, K. B. M. Q. & HUSSAIN, A. K. M. F. 1981 Taylor hypothesis and large-scale coherent structures. *J. Fluid Mech.* **112**, 379–396.